*Journal of Turbulence*
Vol. 13, No. 38, 2012, 1–13



# Energy exchange in an array of vertical-axis wind turbines

Matthias Kinzel*, Quinn Mulligan and John O. Dabiri

*Graduate Aeronautical Laboratories, California Institute of Technology, Pasadena, CA, USA*

(*Received 30 March 2012; final version received 7 July 2012*)

We analyze the flow field within an array of 18 counter-rotating, vertical-axis wind turbines (VAWTs), with an emphasis on the fluxes of mean and turbulence kinetic energy. The turbine wakes and the recovery of the mean wind speed between the turbine rows are derived from measurements of the velocity field using a portable meteorological tower with seven, vertically-staggered, three-component ultrasonic anemometers. The data provide insight to the blockage effect of both the individual turbine pairs within the array and the turbine array as a whole. The horizontal and planform kinetic energy fluxes into the turbine array are analyzed, and various models for the roughness length of the turbine array are compared. A high planform kinetic energy flux is measured for the VAWT array, which facilitates rapid flow recovery in the wake region behind the turbine pairs. Flow velocities return to 95% of the upwind value within six rotor diameters downwind from each turbine pair. This is less than half the recovery distance behind a typical horizontal-axis wind turbine (HAWT). The observed high level of the planform kinetic energy flux is correlated with higher relative roughness lengths for the VAWT array as compared to HAWT farms. This result is especially relevant for large wind farms with horizontal dimensions comparable to the height of the atmospheric boundary layer. As shown in recent work and confirmed here, the planform kinetic energy flux can be the dominant source of energy in such large-scale wind farms.

**Keywords:** wind energy; energy transport; roughness length; turbulence



## 1. Introduction

The flow field in a wind farm is highly complex due to the interaction between the wind turbines and the atmospheric boundary layer. While the fluid mechanics of individual wind turbines are reasonably well understood, their performance is less predictable when situated within a wind farm array. Due to aerodynamic interference between adjacent horizontal-axis wind turbines (HAWTs), in modern wind farms the HAWTs are typically spaced 3–5 rotor diameters, D, apart in the cross-wind direction and 6–10 D apart in the streamwise direction to achieve about 90% of the power output of an isolated HAWT [1, 2]. Recent research even suggests turbine spacings around 15 D for HAWT arrays based on an optimization of the costs per square rotor diameter [3].

To improve the understanding of wind farm aerodynamics, experimental studies have recently been conducted in situ, e.g., at the Horns Rev wind farm in Denmark. In situ measurements are challenging due to the large dimensions of the wind turbines and of the wind farm. The large spatial scales usually limit these investigations to pointwise

*Corresponding author. Email: kinzel@caltech.edu

ISSN: 1468-5248 online only

http://dx.doi.org/10.1080/14685248.2012.712698
http://www.tandfonline.com

velocity measurements with meteorological towers, light detection and ranging (LIDAR), and satellite-based measurement techniques like synthetic aperture radar (SAR) and scatterometry [4, 5]. However, these techniques can be sufficient to qualitatively characterize the wake structures that are created by the individual wind turbines and the wind farm as a whole as well as the power drop between the turbine rows in the downwind direction. Scaled experiments have been performed in wind tunnels for more detailed analyses, by using laboratory-based measurement techniques such as hot wire anemometry, laser Doppler anemometry (LDA), and particle image velocimetry (PIV; see, e.g., [6, 7]). Wind tunnel experiments have the limitation that it is usually not possible to simultaneously match both the Reynolds numbers and the tip speed ratios (i.e., the ratio of blade tip speed to wind speed; TSRs) that occur in a real wind farm setting. Nevertheless they allow for important insights into these flows and are often used to validate numerical results from large eddy simulations (LES) [8, 9]. With the higher spatial resolutions of the wind tunnel experiments and the numerical simulations, it is possible to access not only the flow velocities but also quantities like the Reynolds stresses, dispersive stresses, and fluxes and dissipation of kinetic energy. This data enables investigation of the mechanisms that deliver energy into the wind farm.

The power production of a wind turbine is determined by the kinetic energy flux of the air that moves through the rotor area,

$$P_{\text{horz}} = 0.5\rho A_{\text{rotor}} u^3, \tag{1}$$

where $\rho$ is the density of air, $A_{\text{rotor}}$ the area swept by the rotor, and $u$ the horizontal wind velocity. If $A_{\text{rotor}}$ is replaced with the horizontal projected area of the wind farm, then Equation (1) describes the energy flux entering the wind farm from upwind. This horizontal kinetic energy flux is the dominant source of power for single turbines and small wind farms [8]. For a large wind farm, however, the turbines in the rows located the furthest upwind deplete the horizontal energy flux before it reaches the majority of the turbines. Hence, in large wind farms where the length scale of the wind turbine array exceeds the height of the atmospheric boundary layer ($> 1000 \times 1000\ \text{m}^2$), most of the turbines are supplied by the planform energy flux through the top of the wind turbine array [8]. The planform flux of turbulence kinetic energy can be estimated as [7, 8],

$$P_{\text{vert}} \approx -\rho A_{\text{plan}} u \ <u'w'>, \tag{2}$$

where $A_{\text{plan}}$ is the planform area above the wind turbine array and $<u'w'>$ is the Reynolds shear stress with turbulence velocities $u'$ and $w'$ in horizontal and vertical direction, respectively. Assuming a logarithmic wind velocity profile above the wind farm,

$$u(z) = \frac{u_*}{\kappa}\left[ln\left(\frac{z-d}{z_0}\right)\right], \tag{3}$$

the term $-<u'w'>$ can be expressed as

$$-<u'w'> = u_*^2 = \left[\frac{u\kappa}{ln\left(\frac{z-d}{z_0}\right)}\right]^2. \tag{4}$$

In this equation, $u_*$ is the friction velocity, $\kappa$ the von Karman constant, $\kappa \approx 0.4$, $d$ the zero-plane displacement, which is often approximated by $d \approx 2H/3$, and $z_0$ the roughness length, which is often approximated by $z_0 \approx H/10$, where $H$ is the turbine height (see [10]). Using typical values for current HAWTs of hub height $H = 100$ m and a flow velocity at the hub height of $u = 8\ \mathrm{ms}^{-1}$, the planform kinetic energy flux is approximately $70\ \mathrm{Wm}^{-2}$.

Rather than the rule of thumb $z_0 \approx H/10$, a more precise estimation of the roughness length of HAWT wind farms is often calculated with the Lettau formula [7, 8, 11]:

$$z_{0,\mathrm{Lett}} = 0.5 h^* \frac{s}{S} \tag{5}$$

The Lettau roughness length depends on the height of the roughness elements, $h^*$, the frontal area of the roughness elements, $s$, and the horizontal area per roughness element, $S$. For wind turbines, these values are usually chosen to be $h^* = H$, $s = A_{\mathrm{rotor}}$, and $S = s_x s_y$, where $s_x$ and $s_y$ are the dimensions of the horizontal area per wind turbine. For large HAWTs, typical parameters are a hub height of 100 m, a rotor diameter of 130 m, and a turbine spacing of 10 D in streamwise and 5 D in the transversal direction. This leads to a roughness length of $z_{0,\mathrm{Lett}} \approx 1.5$ m. In comparison, Frandsen [12] developed a formula especially for the calculation of the roughness length of HAWT wind farms:

$$z_{0,\mathrm{Fran}} = z_h \exp\left[-\left(\frac{8\kappa^2 s_x s_y}{\pi C_T}\left[1 - \frac{u_{*lo}^2}{u_{*hi}^2}\right]\right)^{1/2}\right] \tag{6}$$

Similar to the Lettau formula, the Frandsen formula also takes into account the turbine hub height, $z_h = H$, and horizontal area per turbine, $s_x s_y$, but adds turbine-specific parameters, i.e., the friction velocities at the top and bottom of the turbine rotor, $u_{*,hi}$ and $u_{*,lo}$, and the rotor thrust coefficient, $C_T = 4a(1-a)$. Here, $a = 0.5(1 - u_{\mathrm{rear}}/u_{\mathrm{front}})$, where $u_{\mathrm{rear}}$ and $u_{\mathrm{front}}$ are the averaged streamwise velocities downwind and upwind of the wind turbine. The performance of both the Lettau and Frandsen formulae will be evaluated for a VAWT array in this paper.

Calaf et al. [8] report results for LES of a HAWT wind farm with dimensions that scale to a hub height of 100 m, a rotor diameter of 100 m, and a wind farm area of $1000 \times 1000\ \mathrm{m}^2$. They simulated different turbine spacings and derived values for the roughness length between 0.41 m and 8.9 m depending on the geometrical and turbine parameters. The value that they calculated for a turbine spacing comparable to the one used above for the calculation of $z_{0,\mathrm{Lett}}$ is 3.2 m. Inserting the Lettau and the numerically derived roughness length into Equation (4) leads to a planform energy flux of about $21\ \mathrm{Wm}^{-2}$ and $37\ \mathrm{Wm}^{-2}$, respectively, smaller than that derived using the roughness length rule of thumb $z_0 \approx H/10$. Considering the Betz limit (see, e.g., [2]), these values reduce to a maximum power production of approximately $12\ \mathrm{Wm}^{-2}$ and $22\ \mathrm{Wm}^{-2}$ for large wind farms. However, current wind farms have a typical power production of about $2.5\ \mathrm{Wm}^{-2}$, which is approximately a factor of seven smaller than these theoretical values [13]. This brief calculation illustrates that, despite the power coefficients of modern HAWTs approaching the Betz limit, there remains a significant gap between the performance of modern HAWT farms as a whole and the theoretical upper bound given by the planform flux of kinetic energy that supplies the wind farm, the Betz limit notwithstanding.

As an alternative to HAWT farms for converting the planform kinetic energy flux to electricity, here we study an array of counter-rotating VAWTs in a wind farm setting and compare their performance to that of the conventional HAWTs. Previous work by [14, 15]

suggests that wind farms consisting of closely spaced, counter-rotating VAWTs have the potential to achieve an order of magnitude higher power production per unit footprint area than the HAWT equivalent. This paper characterizes the energy transfer into an array of 18 VAWTs, measures horizontal and planform kinetic energy flux, and compares and contrasts the results with conventional HAWT wind farms.

The turbine array and the experimental setup are discussed in the following section. In Section 3, the velocity field, velocity profiles, and energy transfer into the turbine array are presented. Finally, in Section 4, the results are summarized and compared to the aforementioned studies of HAWT wind farms in previous wind tunnel and LES investigations.



## 2. Methods

The VAWT array used in this study is located in the Antelope valley of northern Los Angeles County in California, USA. The location of the array is flat desert terrain for at least 1.5 km in every direction. The mean horizontal wind speed during the measurement campaign was 8.05 $ms^{-1}$ at 10 m, i.e., just above the top of the wind turbine canopy, with a standard deviation of 2.1 $ms^{-1}$. The prevailing wind direction is from the southwest. The probability density function (PDF) of the horizontal velocity during the time of the measurements, 5 July–28 October 2011, is displayed in Figure 1(a) and the corresponding wind rose is given in Figure 1(b). The flow conditions were very similar between the different days of the measurement campaign due to the desert climate. Wind speeds would usually exceed the cut-in speed of the turbines except for the early morning hours. Therefore most of the measurements were taken at times when the atmospheric boundary layer is not neutrally stable, i.e., buoyancy effects contribute to the turbulence levels. The turbines are a commercially available model (Windspire Energy Inc.) with a lift-based rotor design consisting of three airfoils and a 1200-W generator that is connected to the base of the turbine shaft. The turbines have a total height of 9.1 m, a rotor height of 6.1 m, and a diameter of 1.2 m. The cut-in and cut-out speed of the wind turbines are 3.8 $ms^{-1}$ and 12 $ms^{-1}$, respectively. The turbines operate at a nominal rotation rate of 350 rpm and a TSR of 2.3 at a typical inflow velocity of 8 $ms^{-1}$. The turbine parameters are summarized in Table 1.

The layout of the facility is shown in the photograph and sketch in Figures 2(a) and (b), respectively. The turbine array is comprised of a grid of nine counter-rotating turbine pairs

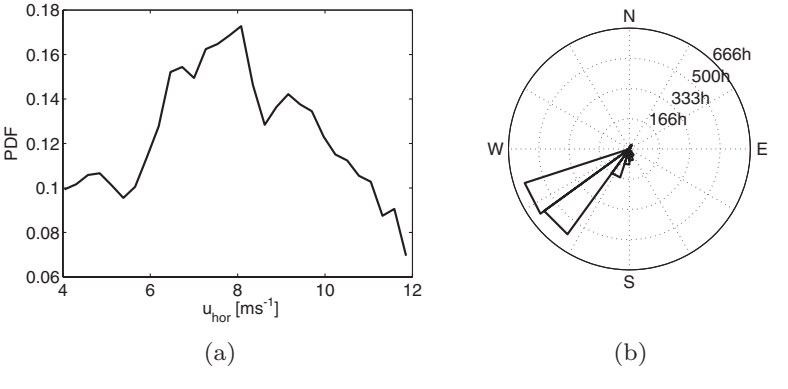


(a) (b)

Figure 1. PDF of the horizontal velocity (a) and wind rose (b) for the time period of the measurements, 5 July–28 October 2011.

Table 1. Turbine parameters.

| Height [m] | Rotor height [m] | D [m] | $s_x$ [D] | $s_y$ [D] | $u_{\text{cut-in}}$ [ms$^{-1}$] | $u_{\text{cut-out}}$ [ms$^{-1}$] | rpm | TSR |
|---|---|---|---|---|---|---|---|---|
| 9.1 | 6.1 | 1.2 | 8 | 8 | 3.8 | 12 | 350 | 2.3 |

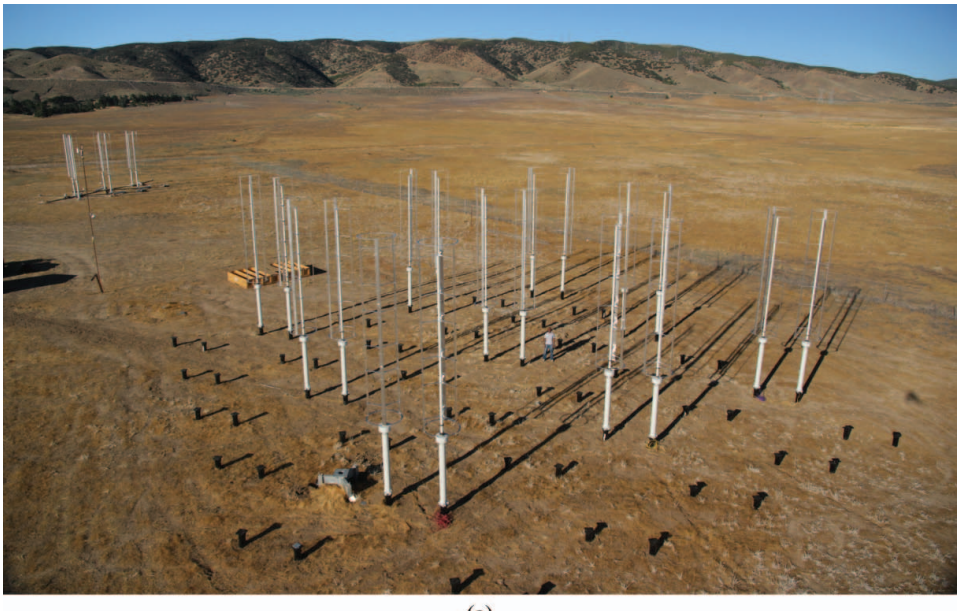

(a)

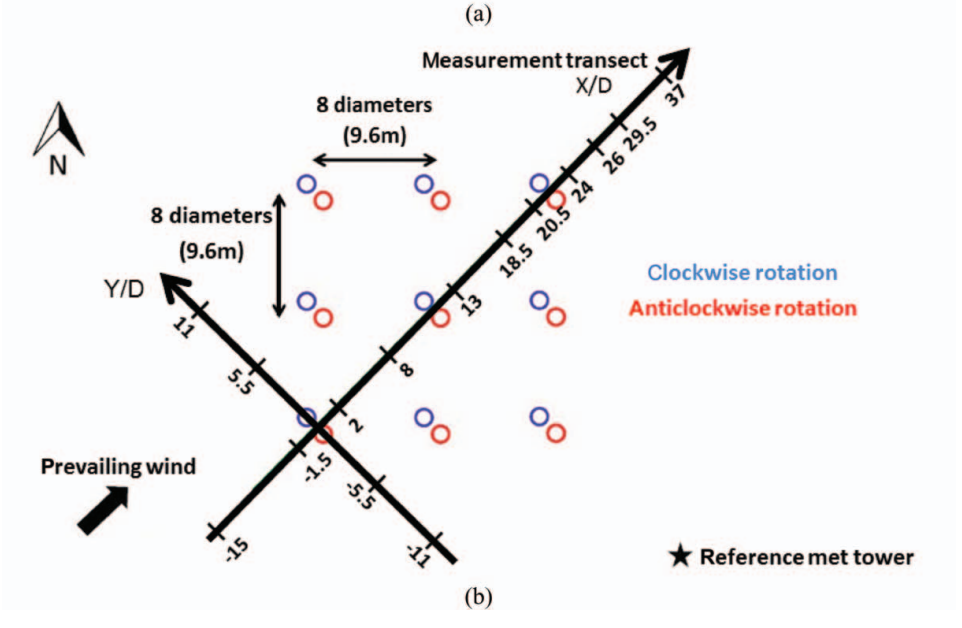


(b)

Figure 2. Photograph (a) and sketch (b) of the VAWT array. Blue circles symbolize clockwise rotating turbines and red circles symbolize anticlockwise rotating turbines. The axis dimensions are given in rotor diameters where D = 1.2 m. The tick marks on the abscissa indicate the measurement locations.

with the turbines in each counter-rotating pair 1.65 D apart from each other. The sense of rotation is such that the turbines rotate into the wind for the prevailing wind direction (see Figure 2(b)). The turbine pairs are arranged on an equidistant grid with distances $s_x = s_y = 8$ D $= 9.6$ m. This baseline configuration was derived from a systematic study of the dependency of the power production of VAWTs on the layout of the turbine locations and the wind direction by [14].

The vertical velocity profiles of the flow were measured at 11 positions along the center line of the turbine array as shown in Figure 2(b). The measurement positions are indicated on the abscissa. For these measurements, seven three-component ultrasonic anemometers (Campbell Scientific CSAT3) were mounted on one 10-m meteorological tower (Aluma-Towers Inc.) and vertically spaced in 1-m increments over the turbine rotor height. Figure 3(a) shows the ultrasonic anemometers mounted to the met tower and their positioning with respect to the turbine rotors. A detailed picture of one of the sensors with the three sensor head pairs visible is shown in Figure 3(b). The CSAT3 sensors were operated at a sampling frequency ($f_{\text{sample}}$) of 10 Hz with a measurement uncertainty of less than 0.161 ms$^{-1}$. Both the sensors and the data logger (Campbell Scientific CR3000) were powered by a solar panel and battery system to make the apparatus fully portable. The tower was moved consecutively to each measurement position along the center line of the turbine array (see measurement transect in Figure 2(b)). The measurement duration at each position was approximately 150 h. This time interval was sufficiently long so as to obtain statistically independent data for the values of the mean and fluctuating velocities.

Because the velocities at the 11 tower positions were not measured simultaneously, the wind speed information from a 10-m reference meteorological tower at the southeast corner of the turbine array was used to condition the data (Figure 2(b)). This anemometer (Thies First Class) recorded data at 1 Hz with an accuracy of ±3%. Using the reference wind data, the measurements from the seven ultrasonic sensors were divided into 10-min time intervals and sorted into bins between 4–6 ms$^{-1}$, 6–8 ms$^{-1}$, 8–10 ms$^{-1}$, and 10–12 ms$^{-1}$


Figure 3. Photograph of a turbine pair with the seven CSAT3 sensors in the background (a) and of one CSAT3 sensor (b). The met-tower for the sensors can be made out behind the left turbine.

Table 2. Measurement parameters.

| $f_{sample}$ [Hz] | Measurement uncertainty [ms$^{-1}$] | Measurement period | Duration per location [h] |
|---|---|---|---|
| 10 | 0.161 | 5 July–28 October 2011 | ≈150 |

depending on the mean velocity information from the reference anemometer. The lower (4 ms$^{-1}$) and upper bound (12 ms$^{-1}$) were chosen to coincide with the cut-in and cut-out speeds of the turbines. Table 2 lists the measurement parameters.

## 3. Results

Averaging the velocities over the seven sensor positions at each measurement location yields the average mean horizontal flow velocity at the rotor midheight. The curve for the averaged mean horizontal flow velocity along the center line of the turbine array is plotted in Figure 4. The measurement transect is plotted on the abscissa and the average of the horizontal velocity over the rotor height on the ordinate. The three turbine pairs along the center line of the turbine array are sketched as vertical bars in the figure at 0 D, 11 D, and 22 D. The error bars show the standard deviation, which is indicative of the turbulence fluctuations at each measurement position. The standard deviation was calculated from all instantaneous velocity measurements. The first measurement point is located 15 D upwind of the wind turbine array where the flow is undisturbed by the presence of the turbines. From this free stream horizontal velocity of 7.2 ms$^{-1}$, the flow slows down to 6.5 ms$^{-1}$ at the position 1.5 D in front of the first turbine pair. This illustrates the blockage effect that the turbine array has on the flow. From the second to the third data point, the velocity drops to 5.1 ms$^{-1}$ over the first turbine pair as the turbines extract energy from the flow. This velocity drop is followed by a recovery to 6.3 ms$^{-1}$ as energy is brought into the turbine array from above and the sides. The energy extraction and recovery cycle repeats itself for the second and third turbine pairs. The velocity to which the flow recovers is lower

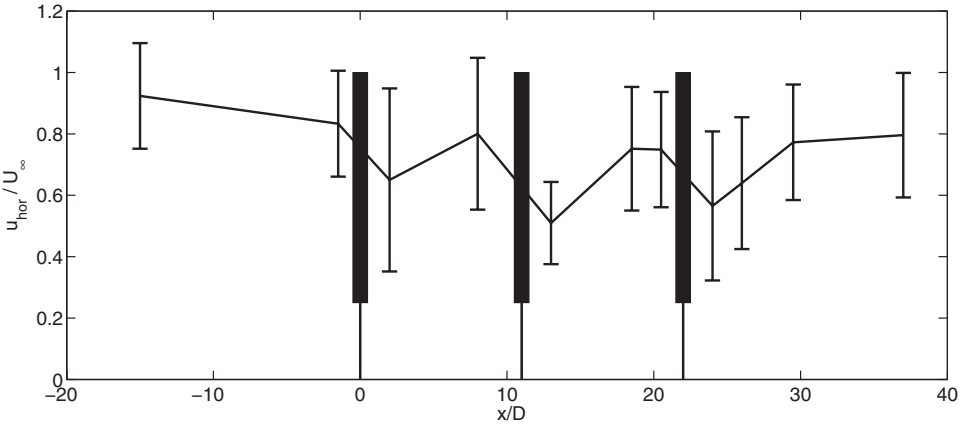


Figure 4. Average mean horizontal flow velocity at rotor midheight normalized by the inflow velocity as measured by the reference anemometer at 10 m plotted over the measurement transect. The three turbine pairs are sketched as vertical bars. The error bars indicate the standard deviation.

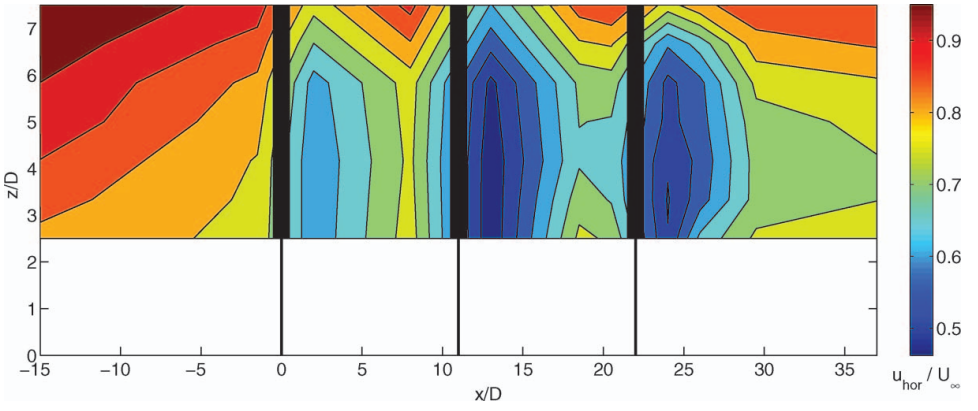


Figure 5. Normalized horizontal velocity contours along the center of the turbine array. The three turbine pairs are indicated by vertical bars.

for the second turbine pair (5.9 $ms^{-1}$) than for the first but stays approximately the same between the second and the third turbine pairs (6.0 $ms^{-1}$). The distance behind a turbine pair required for the flow to recover to 95% of the wind velocity in front of the turbine pair is approximately 6 D. This is larger than the distance of 4 D that was observed by [14], albeit for the wake behind a single VAWT. It is significantly smaller than the 14 D that the flow behind a typical HAWT requires to recover to 95% of the upwind velocity (see [16]). After the third turbine pair, the curve shows the recovery of the flow up to a point 15 D downwind of the turbine array where the horizontal flow velocity is still lower than at the point 1.5 D in front of the turbine array. The two measurement points 3 D and 1.5 D in front of the third turbine pair show how the velocity decreases in front of the turbine pair, which indicates the blockage effect that the individual turbine pairs create in the flow. Therefore, the recovery region does not cover the whole area between two turbine pairs but starts right behind the upwind turbine pair and ends approximately 2 D in front of the downwind turbine pair.

When the data from the seven sensors and the 11 measurement locations are combined, the two-dimensional flow field along the center line of the turbine array is revealed. The normalized horizontal velocities of this flow field are depicted in Figure 5. The measurement transect is presented on the abscissa, the vertical direction on the ordinate, and the horizontal velocity is given as a contour plot. Again, the three turbine pairs are indicated by the black vertical bars at 0 D, 11 D, and 22 D. The two-dimensional horizontal velocity field reveals details regarding the flow around the VAWTs. The highest flow velocities can be found at the top of the wind turbine array as expected. Also, the wake and recovery regions can be clearly made out for the three different turbine pairs. The contours show that the flow velocities drop over the area where the turbine pairs are located as energy is extracted from the flow. Subsequently, the flow velocities start to increase again before the flow interacts with the next turbine pair. The increase in the flow velocities is highest close to the top of the turbines but the recovery is also faster at the bottom of the rotors than at midspan. There is a slight difference in the turbine wake region between the three rows of turbines. The flow velocities remain relatively high after the first row of turbines because the energy transfer from the front and the sides is still dominant in this region of the turbine array. A faster flow recovery can also be seen behind the last row of turbines where there are no turbines located behind or to the sides of the turbine pair. The effect of the absent turbines

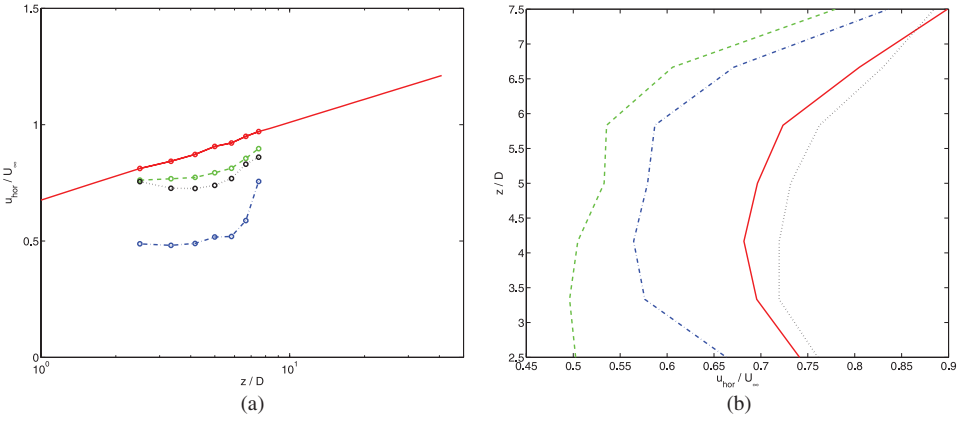


Figure 6. (a) Profiles of the horizontal flow velocity between $0 < z < 40$ D at 15 D (solid) and 1.5 D (dash) upwind and 2 D (dash-dot) and 15 D (dot) downwind of the turbine array. The measurement points are given by markers. (b) Profiles of the horizontal flow velocity over the rotor height 1.5 D (solid) upwind, 2 D (dash), 4 D (dash-dot), and 7.5 D (dash-dot) downwind of the third turbine pair.

behind the last turbine pair becomes most obvious near the top of the wind turbines for $x > 29$ D. However, the flow velocities remain significantly lower behind the turbine array than in the same distance upwind of the turbine array.

The interaction between the turbine array and the atmospheric boundary layer is illustrated in Figure 6(a). The velocity profiles at 15 D (solid line) and 1.5 D (dashed line) upwind of the turbine array as well as 2 D (dash-dotted line) and 15 D (dotted line) downwind of the turbine array are plotted over the vertical distance from the ground. The data on the abscissa is plotted logarithmically. The velocity profile of the atmospheric boundary layer upwind of the turbine array is extrapolated below and above the rotor area with the assumption of a logarithmic profile (see Equation (3)). The estimates $d = 2/3H$ and $z_0 = H/10$ were used to calculate the zero plane displacement and roughness length. For $H$, the average length of the ground vegetation of 0.1 m was applied. The measurement points are given by markers while the interpolated part of the curve does not contain markers. The measurement points fit very well on the curve for the velocity profile of a logarithmic boundary layer. The blockage effect of the turbine array is clearly visible at the measurement location 1.5 D in front of the turbine array. Here, the flow velocities are on average 10% lower in the region of the turbine rotors than they are for the undisturbed velocity profile 15 D upwind of the array. The largest deviation from the undisturbed profile is close to the rotor midspan. This blockage effect is significantly larger for the densely spaced VAWT array than for HAWT wind farms (compare, e.g., [8]). The turbine signature in the horizontal flow velocity profile is more significant at the measurement location 2 D downwind of the turbine array. The flow velocities are about 32% lower compared to the measurement location 1.5 D upwind of the turbine array. The velocity profile 15 D downwind of the turbine array shows the recovery of the flow velocities in the wake of the turbine array. However, the flow velocities only recover to a value of 86% of the flow velocities 15 D upwind of the turbine array and even stay 4% below the flow velocities at the position 1.5 D in front of the turbine array.

Profiles of the horizontal flow velocities over the rotor height are plotted in Figure 6(b) for the measurement positions in the proximity of the third turbine pair. These curves allow analysis of the extraction of energy by the turbine pair as well as the recovery of the flow velocities in the turbine pair's wake. The measurement locations are 1.5 D upwind and 2 D,

4 D, and 7.5 D downwind of the turbine pair. The velocity profiles are presented for the third turbine pair because the most measurement positions are available here. However, the corresponding curves for the second turbine pair are qualitatively similar and vary quantitatively by less than 12.5%. A typical wind profile for the flow in the interior of the wind farm is represented by the velocity profile 1.5 D upwind of the third turbine pair (solid line). The lowest velocity at this location is 5.3 $\mathrm{ms}^{-1}$ and can be found at a position around $1/3H$ from the bottom of the rotor. From there the velocities monotonically increase toward the top and the bottom of the rotor. The velocities are significantly higher at the top than at the bottom of the rotor with values of 7.0 $\mathrm{ms}^{-1}$ and 5.8 $\mathrm{ms}^{-1}$ respectively. The overall velocity profile is due to the higher flow velocities mainly above the turbine canopy but also below the rotor. Energy is transferred from these outer regions into the area of the turbine rotors. The flow is more energetic above the turbine canopy, which results in the higher flow velocities in the upper regions of the rotors. The flow velocities drop on average 1.4 $\mathrm{ms}^{-1}$ to the next measurement position 2 D downwind of the turbine pair. This drop in velocity is equivalent to a loss of kinetic energy and a power extraction from the flow of approximately 1.0 kW based on the frontal area of a turbine pair of VAWTs $A_{2\mathrm{rotors}} = 14.6\ \mathrm{m}^2$ (see Equation (1)). The power density based on the planform area per turbine pair is 11.0 $\mathrm{Wm}^{-2}$. The flow then recovers 0.6 $\mathrm{ms}^{-1}$ on average between 2 D and 4 D and 1 $\mathrm{ms}^{-1}$ between 4 D and 7.5 D behind the turbine pair. This is equivalent to a power recovery of 12.7 $\mathrm{Wm}^{-2}$ based on the planar area of one turbine pair, which provides slightly more energy than the turbine pair extracts. Again, the velocity profiles show the recovery of the flow to a value close to the upwind flow velocity within approximately 6 D.

The mechanisms whereby the energy for the recovery of the flow is transferred into the array of VAWTs can be seen in Figure 7. The planform energy flux per area, $-\rho u < u'w' >$, along the center line of the turbine array is presented as a contour plot. As before, the measurement transect is plotted on the abscissa and the turbine height on the ordinate. The planform energy flux is relatively uniform with a value around 17 $\mathrm{Wm}^{-2}$ in the region upwind of the turbine array. This changes dramatically in the wake of the turbines where energy is transported into the array. The majority of this planform energy flux comes from the top of the turbine canopy. The energy input is especially high in the region 4 D downwind of the turbine pairs and penetrates approximately 1.5 D down from the top into the array. Energy is also injected into the system from below the rotor region. Here, the turbine towers create a wake, which causes higher turbulence intensities and therefore mixing (compare

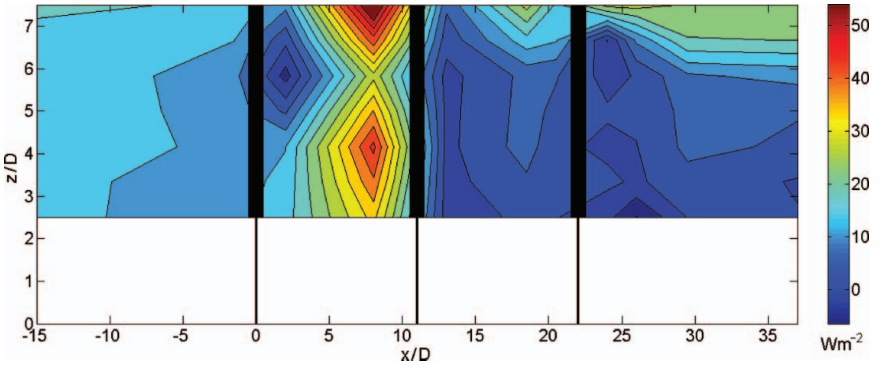


Figure 7. Contours of the power transport due to the planform kinetic energy flux along the center of the turbine array. The three turbine pairs are indicated as vertical bars.

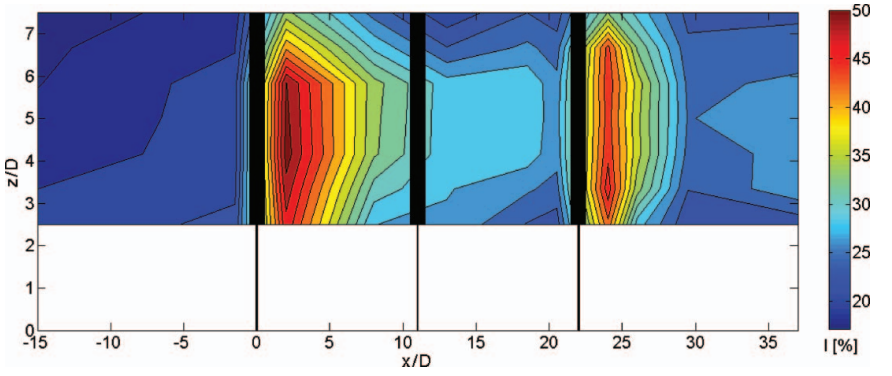


Figure 8. Contours of the turbulence intensity along the center of the turbine array. The three turbine pairs are sketched as vertical structures.

Figure 8). However, this energy transfer is 0.4 $\mathrm{Wm}^{-2}$ on average, which is two orders of magnitude smaller than the one from above the turbine array. Also, its contribution to the total energy flux into the rotor region decreases with increasing size of the wind farm area because the energy below the rotor canopy gets depleted by the turbines located further upwind and does not reach the majority of turbines in the center of large arrays. The regions of high energy transfer agree with the regions of high horizontal velocity in Figure 5. The region behind the first turbine pair stands out because the Reynolds shear stress is a factor of two higher than in the corresponding regions behind the second and third turbine pairs. This indicates a higher level of turbulence in the wake of the first turbine pair in comparison to the other two turbine pairs. This is caused by the interaction of the first turbine pair, which stands exposed in the front of the turbine array and the atmospheric boundary layer. Averaging the planform energy flux for the highest sensor position from 2 D downwind of the second turbine pair to 7.5 D downwind of the third turbine pair results in an average kinetic energy flux into the turbine array of 22 $\mathrm{Wm}^{-2}$. A separate set of measurements collected 0.8 D away from the symmetry axis of the VAWT array show that the energy flux is relatively homogeneous in the region where the turbines are located. But it is to be expected that the turbulence intensity and therefore the planform energy flux are slightly lower in the regions along the lines where the wind does not interact directly with the turbines. However, these regions constitute only 3.8% of the total wind farm area. Therefore, a constant value is assumed for the planform energy flux. With the planform area of $8 \times 8$ D per turbine pair, this leads to a vertical power input of 2.1 kW. This means that the 1.0 kW, which were shown to be extracted by one turbine pair, can be supplied completely by the planform energy flux.

The turbulence intensity along the center of the turbine array is shown as a contour plot in Figure 8. As mentioned above the turbulence intensity is the highest in the turbine wakes with the maximum right behind the rotor.

The roughness length can be estimated by different models, which in turn has an influence on the estimate of the planform energy flux. When the roughness length is estimated by $z_0 \approx H/10 = 0.91$ m, Equation (2) results in a planform energy flux of 42 $\mathrm{Wm}^{-2}$. The values of the roughness length as calculated by the Lettau and Frandsen formulae, Equations (5) and (6), are 0.72 m and 0.13 m, respectively. These formulae lead to a the planform energy flux of 29 $\mathrm{Wm}^{-2}$ and 6 $\mathrm{Wm}^{-2}$ respectively. While the value for the

Table 3. Roughness lengths and vertical energy flux for VAWT and HAWT [4, 8] arrays.

| | $< u_{hor} >$ [ms$^{-1}$] | $u_{hor}$' [ms$^{-1}$] | $z_0$ [m] | $z_{0,Lett}$ [m] | $z_{0,Fran}$ [m] | $P_{z_0}$ [Wm$^{-2}$] | $P_{z_{0,Lett}}$/from LES [Wm$^{-2}$] | $P_{z_{0,Fran}}$ [Wm$^{-2}$] | $P_{measured}$ [Wm$^{-2}$] |
|---|---|---|---|---|---|---|---|---|---|
| VAWT array | 8.05 | 2.1 | 0.91 | 0.72 | 0.13 | 42 | 29 | 6 | 24 |
| HAWT array | 8.4 | | 10 | 1.5 | 3.2 | 71 | 21 | 37 | 2.5 |



planform energy flux as calculated by the Lettau formula lies within 30% of the measured value, the respective values from the estimation and the Frandsen formulae are off by 90% and 75%. These values are summarized in Table 3 and compared to the corresponding values for HAWT arrays.

The total energy that is available inside the wind farm is the sum of the planform energy flux and the power that is transferred into the wind farm from the sides. Taking the wind velocities at the measurement position 1.5 D in front of the first turbine pair as inflow conditions and assuming a logarithmic velocity profile for the area underneath the rotors leads to a horizontal energy flux of 106 Wm$^{-2}$ (see Equation (1)). This is approximately five times the power available from the planform energy flux. With the frontal area per turbine pair of 8 × 7.5 D, this results in a horizontal power transport of 9.2 kW. Only 0.76 kW of this energy is located in the region below the turbine rotor, which supports that this region is less significant for the total energy transfer into the turbine array.

## 4. Conclusions

This experimental field study has analyzed the flow field along the center line of an array of nine pairs of full-scale counter-rotating VAWTs. The velocity field shows the blockage effect of the turbine array as well as the blockage effect of the individual turbine pairs within the array.

The distance behind a turbine pair that the flow needs to recover to 95% of the wind velocity upwind of the turbine pair is approximately 6 D. In comparison, a recovery distance of 4 D was observed by [14] for the wake behind a single VAWT. The distance required for a recovery of the flow velocities is significantly smaller than the 14 D that the flow behind HAWTs needs to recover to 95% of the upwind velocity (see [16]). Hence, pairing the VAWTs may lead to an overall reduction in the average inter-turbine spacing in wind farm arrays.

The horizontal energy flux from the sides is approximately five times higher than the planform energy flux through the top of the turbine canopy. Nevertheless, the planform kinetic energy flux is approximately 15% larger than the energy that the turbines extract from the flow, indicating that it is sufficient to supply energy to the turbines. This is important for large wind farms where the horizontal dimensions exceed that of the atmospheric boundary layer height. The horizontal energy flux will be depleted before it reaches the majority of the turbines in those cases, leaving the planform energy flux as the primary power source. The high planform energy flux in the VAWT array also appears to enable the flow to recover quickly in the wake region behind the turbine pairs. One possible explanation for the relatively high planform kinetic energy flux may be the elevated level of turbulence, which is higher close to the ground than in the regions above where the HAWTs operate. Also, the roughness length of the VAWTs appears to have a stronger influence on the flow,

i.e., increasing the planform energy flux into the turbine array. The roughness length relative to turbine height was observed to be larger for the VAWTs than for typical HAWTs.

The data suggest that the Frandsen formula, which was developed to calculate the roughness length for HAWT wind farms, does not give a good estimate for a VAWT wind farm. The result for the roughness length obtained with the Lettau formula appears to be in better agreement with measurement data. However, the development of a roughness length formula specifically for VAWT arrays is desirable.

The results presented in this paper are dependent on several variables that were not investigated presently, including the turbine spacing and rotational sense, and the specifics of the VAWT design, such as rotor solidity, TSR, thrust coefficient, etc. Ongoing and future work is directed toward determining the dependence of energy exchange on these additional parameters.



**Acknowledgments**

The authors gratefully acknowledge funding from the National Science Foundation Energy for Sustainability program (Grant No. CBET-0725164) and the Gordon and Betty Moore Foundation.

**References**

[1] B. Sørensen, *Renewable Energy: Its Physics, Engineering, Use, Environmental Impacts, Economy, and Planning Aspects*, Elsevier, London, 2004.
[2] E. Hau, *Wind Turbines*, Springer-Verlag, Berlin, 2006.
[3] M. Meyers and C. Meneveau, *Optimal turbine spacing in fully developed wind farm boundary layers*, Wind Energy 15 (2012), pp. 305–317.
[4] C.B. Hasager, R.J. Barthelmie, M.B. Christiansen, M. Nielsen, and S.C. Pryor, *Quantifying offshore wind resources from satellite wind maps: Study area the North Sea*, Wind Energy 9 (2006), pp. 63–74.
[5] M. Méchali, R. Barthelmie, S. Frandsen, L. Jensen, and P.E. Réthoré, *Wake effects at Horns Rev and their influence on energy production*, European Wind Energy Conference and Exhibition, Athens, Greece, 2006.
[6] L.P. Chamorro, R.E.A. Arndt, and F. Sotiropoulos, *Turbulent flow properties around a staggered wind farm*, Bound.-Layer Meteorol. 141 (2011), pp. 349–367.
[7] R.B. Cal, J. Lebrón, L. Castillo, H.S. Kang, and C. Meneveau, *Experimental study of the horizontally averaged flow structure in a model wind-turbine array boundary layer*, Renew. Sust. Energy 2 (2010), 013106.
[8] M. Calaf, C. Meneveau, and J. Meyers, *Large eddy simulation study of fully developed wind-turbine array boundary layers*, Phys. Fluids 22 (2010), 015110.
[9] L.P. Chamorro and F. Porté-Agel, *A wind-tunnel investigation of wind-turbine wakes: Boundary-layer turbulence effects*, Bound.-Layer Meteorol. 132 (2009), pp. 129–149.
[10] J.R. Garratt, *The Atmospheric Boundary Layer*, Cambridge University Press, Cambridge, 1994.
[11] H. Lettau, *Note on aerodynamic roughness-parameter estimation on the basis of roughness-element description*, J. Appl. Meteorol. 8 (1969), pp. 828–832.
[12] S. Frandsen, *On the wind speed reduction in the center of large clusters of wind turbines*, J. Wind Eng. Ind. Aerodyn. 39 (1992), pp. 251–265.
[13] D.J.C. MacKay, *Sustainable Energy – Without the Hot Air*, UIT Cambridge, Cambridge, 2009.
[14] J.O. Dabiri, *Potential order-of-magnitude enhancement of wind farm power density via counter-rotating vertical-axis wind turbine arrays*, J. Renew. Sust. Energy 3 (2011), 043104.
[15] R.W. Whittlesey, S. Liska, and J.O. Dabiri, *Fish schooling as a basis for vertical axis wind turbine farm design*, Bioinsp. Biomim. 5 (2010), 035005.
[16] N. Kelley and B. Jonkman, *A stochastic, full-field, turbulent-wind simulator for use with the AeroDyn-based design codes*, online database (2009). Available at http://wind.nrel.gov/designcodes/preprocessors/turbsim/.